nature communications

Article

https://doi.org/10.1038/s41467-025-57778-7

Amplified multipartite entanglement witnessed in a quantum critical metal

Received: 16 July 2024

Accepted: 26 February 2025

Published online: 14 March 2025

Check for updates

Yuan Fang[1,4], Mounica Mahankali[1,4], Yiming Wang[1,4], Lei Chen[1,4], Haoyu Hu[2], Silke Paschen[3] & Qimiao Si[1]

Strong correlations in matter promote a landscape of quantum phases and associated quantum critical points. For metallic systems, there is increasing recognition that the quantum criticality goes beyond the Landau framework and, thus, further means are needed to characterize the quantum critical fluid. Here we do so by studying an entanglement quantity, the quantum Fisher information, in a strange metal system, focusing on the exemplary case of an Anderson/Kondo lattice model near its Kondo destruction quantum critical point. The spin quantum Fisher information peaks at the quantum critical point and indicates a strongly entangled ground state. Our results are supported by the quantum Fisher information extracted from inelastic neutron scattering measurements in heavy fermion metals. Our work elucidates the loss of quasiparticles in strange metals, opens a quantum information avenue to advance the understanding of metallic quantum criticality in a broad range of strongly correlated systems, and points to a regime of quantum matter to realize amplified entanglement.

Quantum entanglement refers to the entwining of particles such that the quantum state of one cannot be completely described without considering those of the others. This interconnection, lacking a classical counterpart, exhibits unusual properties that defy intuitive understanding[1]. In condensed matter settings, entanglement can play an important role[2]. For example, collective quantum phases of matter in strongly correlated systems, such as the quantum spin liquids and fractional quantum Hall state, are theoretically expected to have strongly entangled ground states[3–5]. Another class of strongly correlated systems are strange metals, which develop near a quantum critical point (QCP). The theory for quantum criticality in such strongly correlated metals goes beyond the Landau framework of order-parameter fluctuations. In the case of heavy fermion metals, a critical destruction of Kondo effect[6–8] has been advanced and extensively evinced[9,10]. As such, their understanding remains a central question[9,11–13]. Because strange metals are also highly collective, it is natural to ask whether a quantum information perspective will allow for progress in understanding.

Here we utilize two quantum information quantities, the mutual information (Fig. 1a) and quantum Fisher information (QFI) (Fig. 1b), to analyze the entanglement behavior near a Kondo destruction QCP (Fig. 1c). While the entanglement entropy (including the mutual information) is an effective measure of entanglement, a protocol of how to experimentally probe it in many-body settings has yet to be established, progress in mesoscopic systems notwithstanding[14,15]. By comparison, the QFI is an entanglement witness. Like the Bell's inequality that determines the bipartite entanglement of qubits from correlation functions[1], the QFI probes the multipartite entanglement in quantum many-body systems[16–20]. We consider the pertinent theoretical model, the Anderson lattice model (see below), and find the QFI of the spin operator to peak at the QCP, with behavior that indicates a strongly entangled ground state. Our results elucidate the anomalous quantum dynamics that are often observed in strange metals.

[1]Department of Physics and Astronomy, Extreme Quantum Materials Alliance, Smalley-Curl Institute, Rice University, Houston, Texas 77005, USA. [2]Department of Physics, Princeton University, Princeton, New Jersey 08544, USA. [3]Institute of Solid State Physics, Vienna University of Technology, Wiedner Hauptstr. 8-10, 1040 Vienna, Austria. [4]These authors contributed equally: Yuan Fang, Mounica Mahankali, Yiming Wang, Lei Chen.
e-mail: qmsi@rice.edu

https://doi.org/10.1038/s41467-025-57778-7

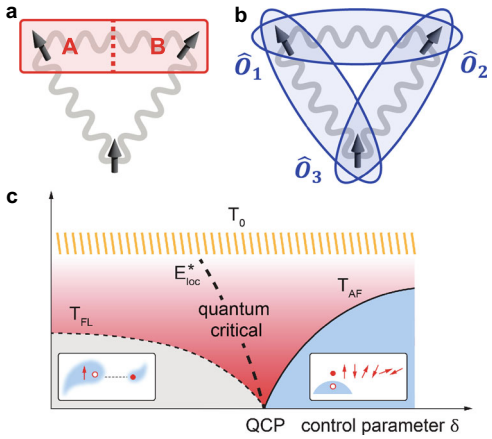

Fig. 1 | Illustration of mutual information, quantum Fisher information and Kondo destruction quantum critical point. a Mutual information that detects the entanglement between two subsystems *A* and *B*. Here the black arrows indicate spins, the gray wavy lines represent entanglement between two spins, the solid red box means the subsystem of interest and the dashed red line is the separation. **b** Quantum Fisher information defined for local operators $\hat{\mathcal{O}}_1, \hat{\mathcal{O}}_2, \hat{\mathcal{O}}_3$ witnesses the multipartite entanglement in the entire system. Here the blue circles represent the correlation of the local operators for the circled two spins. **c** Kondo destruction quantum criticality of a Kondo lattice[13]. Here the control parameter is the ratio of the RKKY coupling to the bare Kondo temperature, $\delta = I/T_K^0$. The Kondo destruction energy scale $E^*_{\rm loc}$ vanishes at the quantum critical point (QCP). The three scales, $T_{\rm AF}$, $T_{\rm FL}$ and T_0 correspond to the temperatures of the AF ordering transition, the crossover into the Fermi liquid and the initial onset of Kondo correlations, respectively. Cartoons on the two sides of the QCP (the boxes) are adapted from ref. 42 where the red arrows are *f* moments and the solid/blank circles represent the particle/hole of *f* electron.

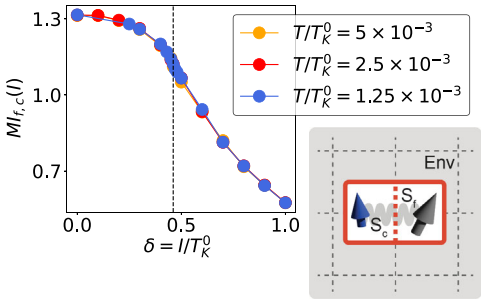

Fig. 2 | Mutual information between the local *f* and *c* electrons. Evolution of the mutual information of local *f* and *c* electrons with the tuning parameter $\delta = I/T_K^0$. The vertical dashed line indicates the QCP. The schematic diagram of this mutual information is depicted on the right bottom corner, where "Env" stands for the rest of the system (the environment). Here, the dashed grids represent the lattice, the red box depicts the impurity subsystem and the red dashed line represents the separation of the *f* and *c* electron spins.

Results

Kondo destruction quantum critical point

The Kondo lattice model—and its strongly-coupled Anderson lattice counterpart—contain two types of degrees of freedom: a lattice of local moments and a band of conduction electrons (see Methods). The spins of the local moments and conduction electrons are coupled by the Kondo interaction, whereas the local moments are coupled by the Rudermana-Kittel-Kasuya-Yosida (RKKY) interaction[6–8,21]. Typically, both types of interactions are antiferromagnetic (AF). The competition between them has been shown[6–8,13] to yield quantum phase transitions that involve a heavy Fermi liquid phase and a Kondo destruction phase (Fig. 1c). In the heavy Fermi liquid phase, where the Kondo coupling wins over the RKKY interaction, the formation of Kondo singlets between the local spins and conduction electrons gives rise to a large Fermi surface. On the other hand, when the RKKY interaction dominates, the correlations among the local spins are detrimental to the formation of any Kondo singlet. As such, at the Kondo destruction QCP where the RKKY and Kondo interactions have the strongest competition, the degree of entanglement among the local spins and conduction electrons represents an intriguing question. The entanglement entropy has been studied in the past for Kondo systems, for models that involve the local moments at the level of either impurity[22–25] or lattice[26]. However, the QCP of the Kondo lattice systems has rarely been characterized by any entanglement means[27].

To set the stage for studying the entanglement properties near the QCP, we start from the mutual information (see Methods) between the local (*f*) and conduction (*c*) electrons:

$$\mathrm{MI}_{f,c} = -S(\hat{\rho}_{f,c}) + S(\hat{\rho}_f) + S(\hat{\rho}_c)\,. \tag{1}$$

Here, $\hat{\rho}_{f,c}$ denotes the density matrix of the *f* and *c* electrons after tracing out the environment (see the schematic in Fig. 2), and $\hat{\rho}_f = \mathrm{tr}_c\,\hat{\rho}_{f,c}$ ($\hat{\rho}_c = \mathrm{tr}_f\hat{\rho}_{f,c}$) is the reduced density matrix of the *f* (*c*) electrons. For definiteness, we consider a square lattice by keeping the nearest neighbor RKKY interaction. Accordingly, the wavevector dependence of the RKKY interaction has the following form: $I_{\mathbf{q}} = I(\cos q_x + \cos q_y)$, where *I* is the strength of the RKKY interaction and (q_x, q_y) is the wavevector at the ordering wavevector $\mathbf{q} = \mathbf{Q} = (\pi, \pi)$, $I_{\mathbf{Q}} = -2I$.

In Fig. 2, we show the evolution of the mutual information ($\mathrm{MI}_{f,c}$) with respect to the non-thermal parameter (δ) that tunes the phase diagram of the Kondo lattice, namely the ratio of the RKKY interaction/to the bare Kondo temperature scale, T_K^0. As this tuning parameter increases, the system undergoes a Kondo destruction quantum phase transition, with the vertical dashed line marking the QCP (cf. Fig. 1c). In the Kondo-screened phase, the mutual information is large, essentially saturating the maximal value $2\ln 2$ of a spin singlet, which is consistent with the local *f* moment being strongly bounded to the conduction electrons. The mutual information is monotonically decreased as the RKKY interaction is increased. Surprisingly, in the Kondo-destroyed side at $\delta > \delta_c$ (cf. Fig. 1c), even though the Kondo singlet is destroyed in the ground state, the mutual information $\mathrm{MI}_{f,c}$ remains nonzero. This result indicates that the Kondo-singlet correlations persist and demonstrates a dynamical Kondo effect[27]. Our result sets the stage to probe quantum entanglement when the QCP is approached from both the Kondo-screened and Kondo-destroyed sides. To do so, we turn to entanglement witness.

Quantum Fisher information—general

The essence of the mutual information is the entanglement between subsystems A and B. A different way to detect such entanglement is by measuring the covariance $\mathrm{tr}((\hat{\rho}_{AB} - \hat{\rho}_A \otimes \hat{\rho}_B)\hat{\mathcal{O}}_A\hat{\mathcal{O}}_B)$ where the Hermitian operator $\hat{\mathcal{O}}_{A/B}$ acts on the A/B subsystem. This correlation witnesses the entanglement between the two subsystems with a proper choice of operators, a notion that has only rarely been considered for condensed matter systems. The QFI corresponds to the summation over all the covariance of site pairs.

Leaving to the Methods and the supplementary information (see Supplementary Note 1) with further details, we note that, on general grounds, the variance is expected to be connected to the correlation functions of the witness operator. Indeed, the QFI of mixed states at temperature *T* can be determined by the dynamical susceptibility of the operator $\hat{\mathcal{O}}$ (ref. 19). Importantly, through the normalized QFI, the bounds of the QFI provide the entanglement content, which is in the same spirit as Bell's inequality.

https://doi.org/10.1038/s41467-025-57778-7

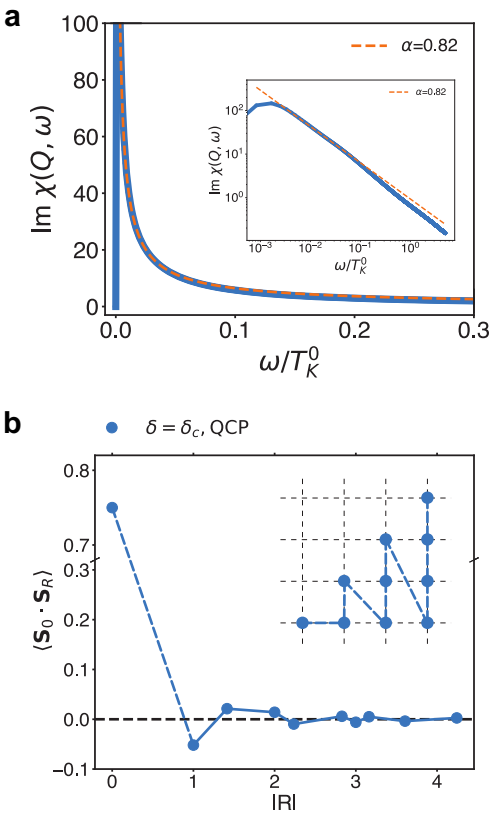

Fig. 3 | Spin-spin correlation functions at the QCP. a The AF dynamical spin susceptibility in real frequency, at the QCP ($\delta = \delta_c$), is obtained by an analytical continuation from $\chi(\mathbf{Q}, i\omega_n)$, which is simulated by the Monte Carlo method. The blue line denotes the $\mathrm{Im}\chi(\mathbf{Q}, \omega)$ at $T/T_K^0 = 2.5\times10^{-3}$ obtained from the Padé decomposition, which peaks in the vicinity of $\omega \sim T$. The lower frequency part of the curve follows a power law scaling with critical exponent $\alpha = 0.82$. The fitting in the log-log plot is presented in the inset. For the fitting, we take the lower limit to be $\omega = 5\times10^{-3}$ (given that the temperature is nonzero) and, for the representative cases of the upper limit 3×10^{-2} and 0.1, we find the r^2 value to be 0.99989671 and 0.99975529, respectively. **b** The equal-time correlation function $\langle \mathbf{S_0}\cdot\mathbf{S_R}\rangle$ at the QCP ($\delta = \delta_c$). Since $|\langle \mathbf{S_0}\cdot\mathbf{S_R}\rangle| < 0.25$ for all $\mathbf{R} \neq 0$, the two-tangle is zero: there is no pairwise entanglement. The inset displays the lattice sites $\mathbf{R}$ we select for the calculation.

Quantum Fisher information near the Kondo destruction quantum critical point

We are now in position to present the results of our calculation on the QFI in the Kondo lattice system. We focus on the spin operator of the f moments at the AF wavevector $\mathbf{Q}$, $\hat{S}^z = \sum_i \hat{S}^z{}_i e^{i\mathbf{Q}\cdot\mathbf{R}_i}$. The normalized QFI density (nQFI) is[19]

$$f_Q = \frac{2}{\pi}\int_{-\infty}^{\infty} \tanh\frac{\omega}{2T}\chi''(\mathbf{Q},\omega)d\omega, \qquad (2)$$

where we set $\hbar = k_B = 1$ (throughout this work) and $\chi''(\mathbf{Q},\omega)$ is the imaginary part of the dynamical spin susceptibility at wave vector $\mathbf{Q}$. [Note that $\chi''(\mathbf{Q},\omega) = \chi''_{S^z}(\omega)/N$, with N the total number of sites.] In practice, the Monte Carlo simulation of the equations in the extended dynamical mean field theory (EDMFT) (see the Methods) is performed on the imaginary frequency axis. We carry out an analytical continuation to obtain the imaginary part of the dynamical spin susceptibility in real frequency, $\chi''(\mathbf{Q},\omega)$ (for details, see Supplementary Note 3). Figure 3a shows $\chi''(\mathbf{Q},\omega)$ at the QCP, which is obtained by a Padé decomposition. The lower-frequency part of the curve follows a power law scaling behavior with an anomalous critical exponent $\alpha \approx 0.82$; its fractional nature is a salient feature of the Kondo destruction QCP[6].

We show the normalized QFI density, at a very low temperature ($T = 2.5\times10^{-3}T_K^0$), versus the tuning parameter $\delta = I/T_K^0$ in Fig. 4a, where the vertical dashed line marks the QCP. The left and right hand sides of the QCP correspond to the Kondo screened phase and Kondo destroyed phase (Fig. 1c), respectively. We find f_Q to display a sharp peak at the QCP, reaching the value around 2.2. This peak exceeds the bound of 2, implying that the ground state contains at least three-partite entanglement according to Eq.(12).

We next fix the system to be at $\delta = \delta_c$ and change the temperature (with the QCP located at $T = 0$). As shown in Fig. 4b, the nQFI monotonically increases with decreasing temperature and reaches the same low-temperature regime of at least three-partite entanglement.

To probe further the entanglement, we compute the two-tangle of spin pairs, which is a measure of the entanglement between two spins[28] (see Supplementary Note 2). At the QCP where the spin parity and translation symmetry are preserved and the magnetic order vanishes, the two-tangle is expressed as $\tau_{0\mathbf{R}} = |\max\{0, -\frac{1}{2} \pm 2\langle \mathbf{S_0}\cdot\mathbf{S_R}\rangle\}|^2$ (refs. 29,30), in which the correlation function $\langle \mathbf{S_0}\cdot\mathbf{S_R}\rangle = \frac{1}{2\pi N_\mathbf{q}}\sum_\mathbf{q} e^{-i\mathbf{q}\cdot\mathbf{R}}\int d\omega\chi(\mathbf{q},\omega)$. Here $N_\mathbf{q}$ is the number of momentum points in the Brillouin zone and $\chi(\mathbf{q},\omega)$ is the dynamical susceptibility of the spin operator.

We present this correlation function in Fig. 3b. It is evident that $\tau_{0\mathbf{R}} = 0$ for every pair of spins. Since our QFI reveals multipartite entanglement in the system, the vanishing two-tangles mean that the entanglement is distributed among multiple spins rather than being confined to pairwise spins. It manifests the quantum monogamy and the Coffman-Kundu-Wootters inequality[31,32]. For example, a maximally entangled state of spins with entanglement distributed among all spins have no entanglement inside any subspace (see Supplementary Note 2; in particular, Supplementary Fig. 1). The combination of a multipartite QFI and vanishing two-tangle provide evidence for strong entanglement in the system.

Finally, to facilitate comparison with inelastic neutron scattering experiments, we show in Fig. 4c, d the (un-normalized) QFI density appropriate for this spectroscopy, viz. for the AF magnetization operator, $g\mu_B\sum_i \hat{S}^z{}_i e^{i\mathbf{Q}\cdot\mathbf{R}_i}$. Here, for an order-of-magnitude estimate of the QFI, we have taken the g-factor to be 2, which is generally considered to be suitable for the 4f crystal field ground state in heavy fermion systems.

Discussion and comparison with experiment

Several points are in order. First of all, our theoretical results at the critical coupling can be tested by experiments. Both the temperature dependence and magnitude of the QFI are supported by the spin QFI we have extracted (see Supplementary Note 4; cf. Supplementary Fig. 2a, compared with Fig. 4d) from the inelastic neutron scattering data[33] of $CeCu_{5.9}Au_{0.1}$; this is a canonical heavy fermion metal in which the Kondo effect is associated with localized spins, as in our model, and it hosts a QCP that has been recognized to be of the Kondo destruction type. Another compound to consider is $Ce_3Pd_{20}Si_6$: Even though the local degrees of freedom here are more complex compared to our model, involving entwined spin and orbital, the QFI result recently determined by inelastic neutron scattering spectroscopy at a field-induced QCP also compares well with our theory (cf. Fig. 3 of ref. 34, compared with Fig. 4d). A further support is that the measured spin dynamics in both materials are singular and have a fractional critical dynamical exponent, as in our theoretical result; the measured exponents are comparable to the theoretical value of $\alpha = 0.82$. In other condensed matter contexts, the QFI has only been measured in several insulating quantum magnets. The low-temperature value for the normalized QFI density we have calculated for the Kondo destruction QCP rises to the values determined in candidate materials for such highly entangled ground states as two-dimensional spin liquids[35,36] (3.4 for $KYbSe_2$, a layered system that realizes a spin-1/2 Heisenberg model on triangle lattice, ref. 30) and one-dimensional spin liquid with

https://doi.org/10.1038/s41467-025-57778-7

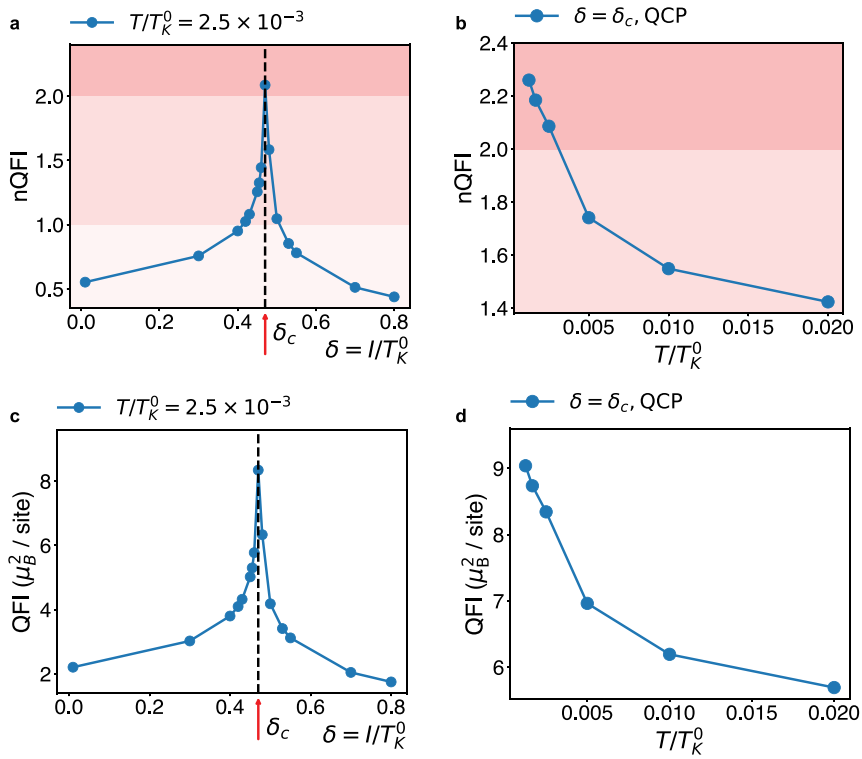

Fig. 4 | The quantum Fisher information density. a The low-temperature normalized QFI density (nQFI) of the AF spin operator, f_Q, as a function of the tuning parameter $\delta = I/T_K^0$. The vertical dashed line and the red arrow indicate the location of the quantum critical point (QCP). The nQFI is peaked at the QCP, where it exceeds 2, indicating that the ground state contains at least three-partite entanglement. The dark (light) red shading, here and in **b**, marks the regime where the system is at least 3- (2-) partite entangled. **b** The nQFI vs. temperature T (normalized by the bare Kondo temperature, T_K^0) at the quantum critical coupling, $\delta_c = I_c/T_K^0$. The results are obtained in the quantum critical regime with $\delta_c = 0.47$, except for the lowest temperature $T = 1.25 \times 10^{-3}$, which requires a finer tuning to reach quantum criticality and is calculated at $\delta_c = 0.465$. **c**, **d** The un-normalized QFI density of the AF magnetization operator, $f_Q(g\mu_B)^2$, suitable for comparison with its inelastic neutron scattering determination. Here, g is taken to be 2.

fractionalized spin excitations (3.8 for $KCuF_3$, a quasi-one-dimensional system that realizes a spin-1/2 Heisenberg chain, ref. 37), respectively. We note that, in our EDMFT calculation, the momentum dependence of the QFI is captured through Eq. (6).

Secondly, we find the QFI to be peaked at the QCP. This result, testable by future experiments on quantum critical heavy fermion systems, establishes the strange metal regime as amplifying quantum entanglement. It is to be contrasted with the observation in certain insulating quantum magnet[38]. Equally important, we find that the multipartite entanglement is witnessed only in the immediate vicinity of the QCP: it no longer is the case when the tuning parameter δ moves outside of the quantum critical regime (Fig. 4a) and the system goes back to the Fermi liquid regime described in terms of quasiparticles (cf. Fig. 1c). Multipartite entanglement is associated with unusual quantum many-body dynamics[39,40]. As such, our work suggests that, in strange metals, multipartite entanglement provides a general characterization of their anomalous dynamics.

More specifically, our work elucidates the key characteristic of strange metallicity, viz. the loss of Landau quasiparticles[13,41]. Our mutual information calculation demonstrates a nearly saturated Kondo entanglement in the paramagnetic (heavy fermion) phase, which describes the formation of Kondo singlets in the ground state (cf. the Supplementary Note 5 and Supplementary Fig. 4a). This implicates a 1-to-1 correspondence: each local moment is converted into a heavy quasiparticle in the excitation spectrum (cf. the Supplementary Fig. 4c, the right part), through the process of breaking up the Kondo singlet (cf. the Supplementary Fig. 4c, the left part). That the calculated mutual information for the Fermi liquid phases leads to pictures consistent with previous intuitive understandings sets the stage for new understandings from the QFI calculation, especially for the strange metal in the quantum critical regime.

The result from our QFI calculation is the development of multipartite entanglement among the *f*-moments in the quantum critical regime. It describes a strong entanglement among the local spins of the resonant-valence-bond (RVB) type (cf. Supplementary Fig. 4d, e), which, through the entanglement monogamy, characterizes the suppression of the *f*-*c* (Kondo) entanglement and, by extension, the strange metal's loss of quasiparticles. This represents a central insight into the inner workings of strange metallicity that is enabled by our study of the quantum Fisher information. Further discussion of this point can be found in Supplementary Note 5.

Our elucidation of the strange metallicity from the entanglement perspective connects well with the existing phenomenology. For example, the QCP of the canonical heavy fermion strange metal $YbRh_2Si_2$ is magnetic (AF, to be precise) in nature, involving a zero-temperature transition between AF and paramagnetic metallic phases. Yet, its charge response is found to be critical[42], a property that also arises in model calculations[43]. The present study implicates an enhanced quantum entanglement as underlying the phenomenon. In turn, our work suggests future studies to probe the QFI of other degrees of freedom that are enabled by the strange metallicity. For example, it is opportune to study the charge QFI from the singular charge fluctuations observed in a cuprate strange metal near optimal superconductivity[44]. Recent proposals for further QFI spectroscopies concern the resonant inelastic X-ray scattering (RIXS)[45,46] and angle-resolved photoemission spectroscopy (ARPES)[47]. Thus, there is considerable prospect for further studies of multipartite entanglement in strange metals.

Summary

We have theoretically studied an entanglement witness in a model for strange metallicity. Our results provide much-needed characterization of beyond-Landau quantum critical metals. The quantum Fisher information reveals amplified entanglement at the quantum critical point. The witnessed multipartite entanglement brings out insights into strange metals' anomalous dynamics and loss of quasiparticles. Our work showcases a window into the quantum correlations that underlie a wide range of strongly interacting metallic systems, and points to broad classes of correlated gapless quantum matter with strange metallicity as a promising setting to witness enhanced entanglement.

Methods

Quantum criticality in the Anderson lattice model

We consider the SU(2) periodic Anderson lattice model, which takes the form:

$$H = \frac{U}{2}\sum_i \left[\sum_\sigma f^\dagger_{i,\sigma} f_{i,\sigma} - 1\right]^2 + \sum_{ij} I_{ij}\mathbf{S}_i \cdot \mathbf{S}_j + V\sum_{i,\sigma}\left(c^\dagger_{i,\sigma} f_{i,\sigma} + f^\dagger_{i\sigma} c_{i,\sigma}\right) + \sum_{p,\sigma}\epsilon_p c^\dagger_{p,\sigma} c_{p,\sigma}\,. \tag{3}$$

Here, $f^\dagger_{i\sigma}$ ($c^\dagger_{i\sigma}$) creates a local (conduction) electron with spin σ at site i. The hybridization V couples the local f-electron with the conduction c-electron, which has a dispersion ϵ_p. Moreover, the on-site Coulomb repulsion is represented by U. When U is sufficiently large, the model is equivalent to the Kondo lattice Hamiltonian, with a Kondo coupling $J_K \sim \frac{4V^2}{U}$. Finally, $\mathbf{S}_i = f^\dagger_i \frac{\boldsymbol{\sigma}}{2} f_i$ represents the spin operator of the local moment at site i, and I_{ij} describes the AF RKKY interaction between the local moments. We consider an RKKY interaction I_{ij}. Its Fourier transformation, $I_{\mathbf{q}}$, reaches the most negative value at the AF wave vector $\mathbf{Q}$, with $I_{\mathbf{Q}} = -2I$.

We treat the Hamiltonian described in Eq. (3) by the extended dynamical mean-field (EDMFT) method, within which the dynamical competition between the Kondo hybridization and RKKY interaction is taken into account appropriately[48–51]. Through EDMFT, the correlation functions of the lattice model are calculated in terms of those of a self-consistent Bose-Fermi Anderson (BFA) model, in which the local f electron couples with a fermionic bath and a bosonic bath. The fermioninc bath comes from the hybridization with the conduction electrons and the bosonic bath describes the spin fluctuations from the RKKY interaction. The action after integrating out both baths takes the form:

$$S_{BFA} = \int_0^\beta d\tau\left[\sum_\sigma f^\dagger_\sigma \partial_\tau f_\sigma + \eta_{\rm loc} S^z + \frac{U}{2}\left(n_f - 1\right)^2\right] - \int_0^\beta d\tau d\tau'\left[\sum_\sigma f^\dagger_\sigma(\tau) V^2 \mathcal{G}_c(\tau-\tau') f_\sigma + \frac{1}{2}\sum_a S^a[\chi_0^{-1}(\tau-\tau')]S^a(\tau')\right], \tag{4}$$

where $\beta = 1/T$ and $n_f = \sum_\sigma f^\dagger_\sigma f_\sigma$. Note, here τ stands for the imaginary time. (Again, we set $\hbar = k_B = 1$ throughout this work). The static Weiss field $\eta_{\rm loc}$ is introduced to capture the AF order, while $\mathcal{G}_c$ and χ_0 denote the Green's function of the fermionic and bosonic bath, respectively. Note that $a \in \{x, y, z\}$. The self-consistent conditions are:

$$\begin{aligned}\chi^a_{\rm loc}(i\omega_n) &= \int d\epsilon \frac{\rho_I(\epsilon)}{\epsilon + M^a(i\omega_n)}\\ M^a(i\omega_n) &= 1/\chi^a_0(i\omega_n) + 1/\chi^a_{\rm loc}(i\omega_n)\\ \mathcal{G}_c(i\omega_n) &= \int d\epsilon \frac{\rho_0(\epsilon)}{-i\omega_n + \epsilon + \Sigma_c(i\omega_n)}\\ \eta_{\rm loc} &= -[2I - \chi^a_0(i\omega_n = 0)]m_{AF}\,.\end{aligned} \tag{5}$$

Here, Σ_c is the conduction-electron self-energy and M^a is the spin cumulant; $\rho_I(\epsilon)$ represents the RKKY density of states, which is obtained from $\rho_I(\epsilon) = \sum_{\mathbf{q}}\delta(\epsilon - I_{\mathbf{q}})$; the subscript "loc" means that quantity is local at the site of an f-moment, and m_{AF} is the AF magnetic moment. We consider a generic density of the conduction electrons (ρ_0) with a nonzero value at the Fermi energy. Finally, the lattice spin susceptibility at momentum $\mathbf{q}$ is calculated by

$$\chi^a(\mathbf{q}, i\omega_n) = \frac{1}{I_{\mathbf{q}} + M^a(i\omega_n)}\,. \tag{6}$$

Mutual information

Mutual information measures the information between two subsystems. Consider a subspace $A \times B \subset M$ where M is the entire manifold of the parameter space of the system, the mutual information of a mixed state $\hat\rho_{AB}$ on this space is defined by[1]

$$\mathrm{MI}(A;B) := S(\hat\rho_A) + S(\hat\rho_B) - S(\hat\rho_{AB}) \tag{7}$$

$$\equiv \mathrm{tr}\left(\hat\rho_{AB}(\ln(\hat\rho_{AB}) - \ln(\hat\rho_A \otimes \hat\rho_B))\right) \tag{8}$$

where $\hat\rho_A = \mathrm{tr}_B\hat\rho_{AB}$, $\hat\rho_B = \mathrm{tr}_A\hat\rho_{AB}$ and $S(\hat\rho) = -\mathrm{tr}(\hat\rho\ln\hat\rho)$ is the von Neumann entropy. In practice, we use the natural logarithm with base e. Note that Eq. (8) is generally applicable for nonzero temperatures as well. The trace is carried out in terms of the local Hilbert space, with each local state contributing a thermally averaged factor. In Fig. 2, we present data for the three lowest temperatures. The data overlap among these temperatures indicates that the temperatures are sufficiently low to capture the behavior of the ground state at zero temperature.

Quantum Fisher information

To pave the way for the calculations presented in this work, we motivate how summing over all the covariance of site pairs leads to the QFI, and elaborate on how the QFI can witness the multipartite entanglement and be measured in experiments. Specifically, we consider the z-component of the f-spin operators of the Kondo lattice.

The clearest case arises in a pure state, for which the QFI is defined as the variance function $F_Q = 4\mathrm{Var}(\hat S^z) \equiv 4(\langle(\hat S^z)^2\rangle - \langle\hat S^z\rangle^2)$ (see Supplementary Note 1). Consider a lattice comprising N sites, and the operator $\hat S^z = \sum_{i=1}^N \hat S^z{}_i$ where the operator $\hat S^z{}_i$ acts only on site i. We find (as derived in Supplementary Note 1) that the QFI is written as follows:

$$\frac{F_Q}{4} = \sum_{i=1}^N \mathrm{Var}(\hat S^z{}_i) + \sum_{i,j\neq i}\mathrm{tr}\left(\left(\hat\rho_{ij} - \hat\rho_i\otimes\hat\rho_j\right)\hat S^z{}_i \otimes \hat S^z{}_j\right) \tag{9}$$

where $\hat\rho_i = \mathrm{tr}_{j\neq i}\hat\rho$ and $\hat\rho_{ij} = \mathrm{tr}_{l\neq i,j}\hat\rho$. The second term in Eq. (9) measures the difference between $\hat\rho_{ij}$ and $\hat\rho_i \otimes \hat\rho_j$ which is non-vanishing if the states on site i and j are entangled. We recognize that the mutual information captures the difference between $\ln(\hat\rho_{ij})$ and $\ln(\hat\rho_i \otimes \hat\rho_j)$ (See Eq. (8)). Thus, the QFI measures the sum of pairwise entanglement between all pairs of sites, which contains the information of multipartite entanglement.

For calculations at nonzero temperatures, we consider the case of a mixed state $\hat\rho$. The QFI is defined for the Hermitian operator $\hat S^z$ with the spectral decomposition $\hat\rho = \sum_{\lambda_n}\lambda_n|\lambda_n\rangle\langle\lambda_n|$, it is expressed as[18,19]

$$F_Q = 2\sum_{nm}\frac{(\lambda_n - \lambda_m)^2}{\lambda_n + \lambda_m} S^z_{nm} S^z_{mn}. \tag{10}$$

where $S^z_{nm} = \langle\lambda_n|\hat S^z|\lambda_m\rangle$. Further details about the QFI are introduced in Supplementary Note 1. The QFI of mixed states at temperature T is

determined by the susceptibility of operator $\widehat{S^z}$ (ref. 19) via

$$F_Q = \frac{2}{\pi}\int_{-\infty}^{\infty} \tanh\frac{\omega}{2T}\chi''(\omega)d\omega\,, \tag{11}$$

where $\chi''(\omega)$ is the imaginary part of the susceptibility $\chi(\omega) = i\int_0^\infty dt e^{i\omega t}\mathrm{tr}\left(\hat{\rho}[\widehat{S^z}(t), \widehat{S^z}(0)]\right)$.

QFI bounds from the normalized QFI

Assume $\widehat{\mathcal{O}} = \sum_{i=1}^{N}\widehat{\mathcal{O}}_i$ and a mixed state of dimension N where $\widehat{\mathcal{O}}_i$ acts on the i-th particle (basis vector). If the ground state can be written as the product of some k-partite entangled states with $k \le m$, the QFI density $f_Q = F_Q/N$ is bounded above by: $f_Q \le m(h_{\max} - h_{\min})^2$, where $h_{\max/\min}$ is the maximal/minimal eigenvalue of the operator $\widehat{\mathcal{O}}_i$ (for a version of the proof, see Supplementary Note 1. Consequently, if

$$f_Q > m(h_{\max} - h_{\min})^2, \tag{12}$$

it witnesses the existence of at least $m+1$-partite entangled states in the system[16]. In the remainder of this work, we focus on spin-1/2 systems. Here, we consider the f-spin operator of a Kondo lattice (an Anderson lattice at sufficiently large U), and the maximal and minimal eigenvalues are $h_{\max} = 1/2$ and $h_{\min} = -1/2$. Then the normalized QFI density, nQFI, is $f_Q/(h_{\max} - h_{\min})^2 = f_Q$.

Data availability

The data that support the findings of this study are either presented in the manuscript or available at https://doi.org/10.5281/zenodo.14814713.

Code availability

The computer codes that were used to generate the data that support the findings of this study are available from the corresponding author upon request.

References

1. Nielsen, M. A. & Chuang, I. L.*Quantum computation and quantum information* https://doi.org/10.1017/CBO9780511976667 (Cambridge university press, 2010).
2. Amico, L., Fazio, R., Osterloh, A. & Vedral, V. Entanglement in many-body systems. *Rev. Mod. Phys.* **80**, 517–576 (2008).
3. Wen, X.-G.*Quantum field theory of many-body systems: from the origin of sound to an origin of light and electrons* https://doi.org/10.1093/acprof:oso/9780199227259.001.0001 (OUP Oxford, 2004).
4. Kitaev, A. & Preskill, J. Topological entanglement entropy. *Phys. Rev. Lett.* **96**, 110404 (2006).
5. Li, H. & Haldane, F. D. M. Entanglement spectrum as a generalization of entanglement entropy: Identification of topological order in non-abelian fractional quantum hall effect states. *Phys. Rev. Lett.* **101**, 010504 (2008).
6. Si, Q., Rabello, S., Ingersent, K. & Smith, J. L. Locally critical quantum phase transitions in strongly correlated metals. *Nature* **413**, 804–808 (2001).
7. Coleman, P., Pépin, C., Si, Q. & Ramazashvili, R. How do fermi liquids get heavy and die? *J. Phys.: Condens. Matter* **13**, R723 (2001).
8. Senthil, T., Vojta, M. & Sachdev, S. Weak magnetism and non-fermi liquids near heavy-fermion critical points. *Phys. Rev. B* **69**, 035111 (2004).
9. Paschen, S. & Si, Q. Quantum phases driven by strong correlations. *Nat. Rev. Phys.* **3**, 9–26 (2021).
10. Kirchner, S., Paschen, S., Chen, Q., Wirth, S., Feng, D., Thompson, J. D. & Si, Q. Colloquium: Heavy-electron quantum criticality and single-particle spectroscopy. *Rev. Mod. Phys.* **92**, 011002 (2020).
11. Coleman, P. & Schofield, A. J. Quantum criticality. *Nature* **433**, 226–229 (2005).
12. Phillips, P. W., Hussey, N. E. & Abbamonte, P. Stranger than metals. *Science* **377**, eabh4273 (2022).
13. Hu, H., Chen, L. & Si, Q. Quantum critical metals and loss of quasiparticles. *Nat. Phys.* **20**, 1863–1873 (2024).
14. Islam, R. et al. Measuring entanglement entropy in a quantum many-body system. *Nature* **528**, 77–83 (2015).
15. Klich, I. & Levitov, L. Quantum noise as an entanglement meter. *Phys. Rev. Lett.* **102**, 100502 (2009).
16. Hyllus, P. et al. Fisher information and multiparticle entanglement. *Phys. Rev. A* **85**, 022321 (2012).
17. Tóth, G. Multipartite entanglement and high-precision metrology. *Phys. Rev. A* **85**, 022322 (2012).
18. Liu, J., Yuan, H., Lu, X.-M. & Wang, X. Quantum fisher information matrix and multiparameter estimation. *J. Phys. A: Math. Theor.* **53**, 023001 (2019).
19. Hauke, P., Heyl, M., Tagliacozzo, L. & Zoller, P. Measuring multipartite entanglement through dynamic susceptibilities. *Nat. Phys.* **12**, 778–782 (2016).
20. Scheie, A., Laurell, P., Dagotto, E., Tennant, D. A. & Roscilde, T. Reconstructing the spatial structure of quantum correlations in materials. *Phys. Rev. Res.* **6**, 033183 (2024).
21. Hewson, A. C.*The Kondo problem to heavy fermions* https://doi.org/10.1017/CBO9780511470752 (Cambridge university press, 1997).
22. Wagner, C., Chowdhury, T., Pixley, J. H. & Ingersent, K. Long-range entanglement near a kondo-destruction quantum critical point. *Phys. Rev. Lett.* **121**, 147602 (2018).
23. Bayat, A., Bose, S., Sodano, P. & Johannesson, H. Entanglement probe of two-impurity kondo physics in a spin chain. *Phys. Rev. Lett.* **109**, 066403 (2012).
24. Bayat, A., Sodano, P. & Bose, S. Negativity as the entanglement measure to probe the kondo regime in the spin-chain kondo model. *Phys. Rev. B* **81**, 064429 (2010).
25. Alkurtass, B. et al. Entanglement structure of the two-channel kondo model. *Phys. Rev. B* **93**, 081106 (2016).
26. Parisen Toldin, F., Sato, T. & Assaad, F. F. Mutual information in heavy-fermion systems. *Phys. Rev. B* **99**, 155158 (2019).
27. Hu, H., Cai, A. & Si, Q. Quantum Criticality and Dynamical Kondo Effect in an SU(2) Anderson Lattice Model. *arXiv e-prints* arXiv:2004.04679 https://doi.org/10.48550/arXiv.2004.04679 (2020).
28. Wootters, W. K. Entanglement of formation of an arbitrary state of two qubits. *Phys. Rev. Lett.* **80**, 2245–2248 (1998).
29. Amico, L., Osterloh, A., Plastina, F., Fazio, R. & Massimo Palma, G. Dynamics of entanglement in one-dimensional spin systems. *Phys. Rev. A* **69**, 022304 (2004).
30. Scheie, A. O. et al. Proximate spin liquid and fractionalization in the triangular antiferromagnet $KYbSe_2$. *Nat. Phys.* **20**, 74–81 (2024).
31. Coffman, V., Kundu, J. & Wootters, W. K. Distributed entanglement. *Phys. Rev. A* **61**, 052306 (2000).
32. Osborne, T. J. & Verstraete, F. General monogamy inequality for bipartite qubit entanglement. *Phys. Rev. Lett.* **96**, 220503 (2006).
33. Schröder, A. et al. Onset of antiferromagnetism in heavy-fermion metals. *Nature* **407**, 351–355 (2000).
34. Mazza, F. et al. Quantum Fisher information in a strange metal. *arXiv e-prints* https://arxiv.org/pdf/2403.12779.pdf (2024).
35. Mathew, G. et al. Experimental realization of multipartite entanglement via quantum fisher information in a uniform antiferromagnetic quantum spin chain. *Phys. Rev. Res.* **2**, 043329 (2020).
36. Pratt, F. L., Lang, F., Steinhardt, W., Haravifard, S. & Blundell, S. J. Spin dynamics, entanglement, and the nature of the spin liquid state in $ybzngao_4$. *Phys. Rev. B* **106**, L060401 (2022).
37. Scheie, A. et al. Witnessing entanglement in quantum magnets using neutron scattering. *Phys. Rev. B* **103**, 224434, https://doi.org/10.1103/PhysRevB.107.059902 (2021).

38. Laurell, P. et al. Quantifying and controlling entanglement in the quantum magnet cs_2cocl_4. *Phys. Rev. Lett.* **127**, 037201 (2021).
39. Brenes, M., Pappalardi, S., Goold, J. & Silva, A. Multipartite entanglement structure in the eigenstate thermalization hypothesis. *Phys. Rev. Lett.* **124**, 040605 (2020).
40. Smith, J. et al. Many-body localization in a quantum simulator with programmable random disorder. *Nat. Phys.* **12**, 907–911 (2016).
41. Chen, L. et al. Shot noise in a strange metal. *Science* **382**, 907–911 (2023).
42. Prochaska, L. et al. Singular charge fluctuations at a magnetic quantum critical point. *Science* **367**, 285–288 (2020).
43. Cai, A., Yu, Z., Hu, H., Kirchner, S. & Si, Q. Dynamical scaling of charge and spin responses at a kondo destruction quantum critical point. *Phys. Rev. Lett.* **124**, 027205 (2020).
44. Mitrano, M. et al. Anomalous density fluctuations in a strange metal. *Proc. Natl Acad. Sci.* **115**, 5392–5396 (2018).
45. Hales, J. et al. Witnessing light-driven entanglement using time-resolved resonant inelastic x-ray scattering. *Nat. Commun.* **14**, 3512 (2023).
46. Baykusheva, D. R. et al. Witnessing nonequilibrium entanglement dynamics in a strongly correlated fermionic chain. *Phys. Rev. Lett.* **130**, 106902 (2023).
47. Malla, R. K., Weichselbaum, A., Wei, T.-C. & Konik, R. M. Detecting Multipartite Entanglement Patterns using Single Particle Green's Functions. *arXiv e-prints* arXiv:2310.05870 https://doi.org/10.48550/arXiv.2310.05870 (2023).
48. Hu, H., Chen, L. & Si, Q. Extended Dynamical Mean Field Theory for Correlated Electron Models. *arXiv e-prints* arXiv:2210.14197 https://doi.org/10.48550/arXiv.2210.14197 (2022).
49. Si, Q. & Smith, J. L. Kosterlitz-thouless transition and short range spatial correlations in an extended hubbard model. *Phys. Rev. Lett.* **77**, 3391–3394 (1996).
50. Smith, J. L. & Si, Q. Spatial correlations in dynamical mean-field theory. *Phys. Rev. B* **61**, 5184–5193 (2000).
51. Chitra, R. & Kotliar, G. Effect of long range coulomb interactions on the mott transition. *Phys. Rev. Lett.* **84**, 3678–3681 (2000).

Acknowledgments

We thank Gabriel Aeppli, Fakher Assaad, Matthew Foster, Pontus Laurell, Matteo Mitrano, Han Pu, Allen Scheie, Oliver Stockert and Alan Tennant for useful discussions. Work at Rice has primarily been supported by the the NSF Grant No. DMR-2220603 (Y.F.), the AFOSR Grant No. FA9550-21-1-0356 (M.M.,Y.W.) the Robert A. Welch Foundation Grant No. C-1411 (L.C.), and the Vannevar Bush Faculty Fellowship ONR-VB N00014-23-1-2870 (Q.S.). The majority of the computational calculations have been performed on the Shared University Grid at Rice funded by NSF under Grant EIA-0216467, a partnership between Rice University, Sun Microsystems, and Sigma Solutions, Inc., the Big-Data Private-Cloud Research Cyberinfrastructure MRI-award funded by NSF under Grant No. CNS-1338099, and the Extreme Science and Engineering Discovery Environment (XSEDE) by NSF under Grant No. DMR170109. H.H. acknowledges the support of the European Research Council (ERC) under the European Union's Horizon 2020 research and innovation program (Grant Agreement No. 101020833). Work in Vienna was supported by the Austrian Science Fund (projects I 5868-N - FOR 5249 - QUAST, SFB F 86, Q-M&S, and 10.55776/COE1, quantA) and the ERC (Advanced Grant CorMeTop, No. 101055088). Several of us (Y.F., M.M., Y.W., L.C., S.P., Q.S.) acknowledge the hospitality of the Kavli Institute for Theoretical Physics, supported in part by the National Science Foundation under Grant No. NSF PHY1748958, during the program "A Quantum Universe in a Crystal: Symmetry and Topology across the Correlation Spectrum". Q.S. and S.P. acknowledge the hospitality of the Aspen Center for Physics, which is supported by NSF grant No. PHY-2210452.

Author contributions

Q.S. conceived the research. Y.F., M.M., Y.W., L.C., H.H. and Q.S. carried out model studies. Y.F., Y.W., S.P. and Q.S. contributed to the comparison of our calculated QFI with experimental measurements. Y.F., M.M., Y.W., L.C. and Q.S. wrote the manuscript, with inputs from all authors.

Competing interests

The authors declare no competing interests.

Additional information

Supplementary information The online version contains supplementary material available at https://doi.org/10.1038/s41467-025-57778-7.

Correspondence and requests for materials should be addressed to Qimiao Si.

Peer review information *Nature Communications* thanks Yashar Komijani, Yao Wang, and the anonymous, reviewers, for their contribution to the peer review of this work. A peer review file is available.